

## Electronic bipolar resistance switching in an anti-serially connected Pt/TiO<sub>2</sub>/Pt structure for improved reliability

This article has been downloaded from IOPscience. Please scroll down to see the full text article.

2012 Nanotechnology 23 035201

(<http://iopscience.iop.org/0957-4484/23/3/035201>)

View [the table of contents for this issue](#), or go to the [journal homepage](#) for more

Download details:

IP Address: 147.46.237.119

The article was downloaded on 17/12/2011 at 01:35

Please note that [terms and conditions apply](#).

# Electronic bipolar resistance switching in an anti-serially connected Pt/TiO<sub>2</sub>/Pt structure for improved reliability

Kyung Min Kim, Seungwu Han and Cheol Seong Hwang

WCU Hybrid Materials Program, Department of Materials Science and Engineering and Inter-University Semiconductor Research Center, Seoul National University, Seoul 151-744, Korea

E-mail: [cheolsh@snu.ac.kr](mailto:cheolsh@snu.ac.kr)

Received 15 September 2011, in final form 3 November 2011

Published 16 December 2011

Online at [stacks.iop.org/Nano/23/035201](http://stacks.iop.org/Nano/23/035201)

## Abstract

Electronic bipolar resistive switching and its degradation in the Pt/TiO<sub>2</sub>/Pt structure were studied. The electronic bipolar switching was induced from the asymmetric trap distribution of the structure under its unipolar reset state. The imbalanced migration of oxygen accompanied by electronic switching significantly degrades switching endurance. Instead, the anti-serial connection of Pt/TiO<sub>2</sub>/Pt cells resulted in substantial improvements in endurance, underscoring the importance of vacancy migration in device reliability. In addition, the independent control of resistance states of the two connected cells provides the freedom to control resistance ratio, switching direction, and reliability.

(Some figures may appear in colour only in the online journal)

## 1. Introduction

High density solid-state non-volatile memory (NVM) devices are key components in every modern computer. Resistance switching (RS) random access memory (ReRAM) has attracted a great deal of interest as a promising NVM device aiming at replacing charge-based flash memory [1–3]. RS systems can be broadly classified into two categories: ionic switching and electronic switching systems. Ionic switching is induced by a thermochemical reaction, valence change, or electrochemical reaction [2], while the electronic switching is almost exclusively performed by electronic carrier trapping/detrapping. Even though these two switching types have been believed to have quite distinctive origins and, thus, are realized in different material systems, the close correlation between them is becoming known and their simultaneous appearance has been reported from a single material system. TiO<sub>2</sub> is one of several systems that show both types of RS behavior; it is a typical thermochemical ionic RS material but also shows electronic RS under certain circumstances [4–7]. The first report on the simultaneous presence of these two types of RS in TiO<sub>2</sub> was made by Jeong *et al* [5], and the electronic nature of the bipolar

electronic RS that was induced from the reset state of unipolar filamentary ionic switching was recently elucidated in detail by Kim *et al* [7, 8]. Electronic bipolar RS corresponds to a case in which trap-mediated hysteretic electronic conduction is asymmetric with respect to the bias polarity [7]. The origin of the asymmetry was ascribed to the presence of an asymmetric potential barrier ( $\Phi_{\text{asym}}$ ) between the trap and the trap-free regions in the local region near the anode in which the conducting filament (CF) ruptured during the unipolar ionic reset step. Within this context, the set and reset switching was understood as the trap filling and emptying processes, respectively, where the abrupt set switching was ascribed to the trap filling limit (TFL) of conventional space-charge-limited conduction (SCLC) behavior [7].

Electronic switching could generally have better RS performance considering the easier motion of electronic carriers compared to ionic species (oxygen ions or metal ions such as Cu or Ag). However, the experimental results are not necessarily consistent with this general conjecture. In addition, ionic motion during electronic switching, which may interfere with the electronic RS, cannot be completely excluded. In this work, the origin of the degradation of the

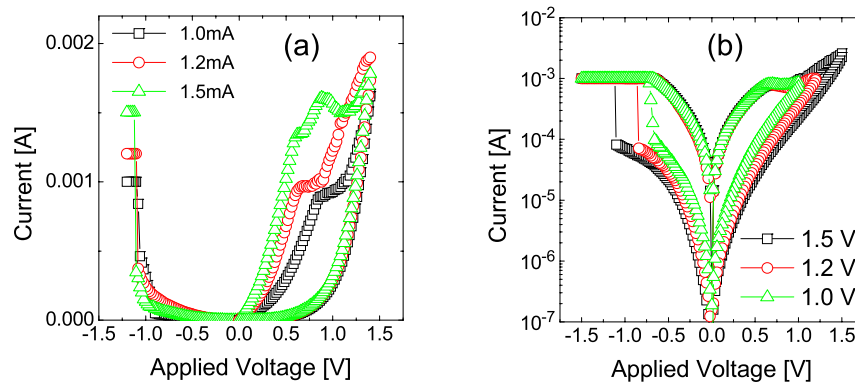


**Figure 1.** Typical bipolar current–voltage switching curves in (a) linear and (b) semi-log scale obtained from the same resistance switching cells with different compliance currents for set switching under negative bias and different maximum reset positive voltages.

electronic bipolar RS is examined, and a method to improve the degradation is suggested.

## 2. Experimental procedure

A 60 nm thick  $\text{TiO}_2$  thin film was deposited on a 100 nm thick sputtered Pt/ $\text{SiO}_2$ /Si substrate by plasma-enhanced atomic layer deposition at 250 °C using Ti tetraisopropoxide as the precursor and plasma-activated  $\text{O}_2$  as the oxidant [4]. Structural and chemical characterizations using x-ray diffraction and x-ray photoelectron spectroscopy showed that the as-grown  $\text{TiO}_2$  film has a polycrystalline anatase structure with an O/Ti ratio of  $\sim 2.1$ . The grain shape was columnar and no specific preferred crystallographic orientation was observed. A 50 nm thick circular shaped Pt top electrode with a 100  $\mu\text{m}$  diameter was then fabricated by electron beam evaporation followed by a lift-off photolithographic process. The resistive switching behavior of the films was measured at room temperature using a Hewlett Packard 4145B semiconductor parameter analyzer, an Agilent 81110A current pulse generator, and a Tektronix TDS 684C oscilloscope. The switching behavior of a single metal–insulator–metal (MIM) sample was measured by application of a bias voltage to the top electrode (TE), while the bottom electrode (BE) was grounded. Serially connected MIM–MIM samples were also measured by application of a bias voltage between two adjacent TEs.

## 3. Results and discussion

The MIM sample showed a typical unipolar RS after the sample was electroformed initially. The sample was then set to the unipolar reset state by a current–voltage ( $I$ – $V$ ) sweep, which generally corresponds to the bipolar set state due to the carrier-filled configuration of traps in the following bipolar RS. The sample can then be switched to the bipolar reset state by application of a positive bias to the TE. The sample returns to the bipolar set state when the negative bias is applied to the TE while the compliance current (CC) is limited to  $\lesssim 5$  mA. When the CC is increased to  $\gtrsim 10$  mA, the sample returns to the unipolar set state by rejuvenation of

the partially ruptured CF, which is made up of Magnéli phases ( $\text{Ti}_n\text{O}_{2n-1}$ , where  $n =$  typically 4–5) in a  $\text{TiO}_2$  system [3, 9]. Therefore, in this study, a  $\text{CC} < 5$  mA was always maintained. Figures 1(a) and (b) show the typical bipolar  $I$ – $V$  switching curves ((a) and (b) in linear and semi-log scales, respectively) obtained from the same RS cell with different CC for the set switching under the negative bias and different maximum reset positive voltages, respectively. When the Magnéli phase CF was ruptured during the unipolar reset process, mostly by the Joule heating effect [3, 9], the local reset region near the anode was composed of discrete electron traps, the density of which is dependent on the transient conditions during the unipolar set and reset switching [7]. While the trap density appears to play a crucial role in determining whether the character of subsequent bipolar switching is electronic (SCLC mechanism) or ionic (valence change mechanism; Schottky barrier modulation), the factors that determine the remaining trap density are not well understood yet. It can be noted that the shapes of the BRS curves shown in figure 1 are quite similar to those in other reports where the valence change type ionic switching is attributed as the ruling mechanism [10]. This makes the clarification of whether it is of electronic or ionic nature not trivial. This aspect was discussed in detail in [7], and it was confirmed that SCLC is the dominant current conduction mechanism supporting the electronic nature of the switching in this specific case.

The possible reason for the occurrence of electronic BRS in one case and ionic BRS in the other case is discussed a little more below. When the concentration of defects (mostly oxygen vacancies) in the dielectric film near the electrode is very high ( $\gtrsim 10^{20}$ – $10^{21}$   $\text{cm}^{-3}$ ), the interfacial Schottky potential barrier height becomes quite low ( $\lesssim 0.1$  eV), allowing fluent carrier injection into the conduction band of the insulator. Due to the presence of high density defects and limited carrier mobility in the dielectric layer, the carriers experience a charge accumulation effect, which enables the SCLC mechanism to appear. In this case, the low resistance of the insulator layer does not allow a high electric field, a requirement to induce the movement of ionic defects, to be applied over the layer so that it is hard for an ionic switching mechanism to be achieved. On the other hand, if the initial defect density is relatively low, a higher Schottky barrier can

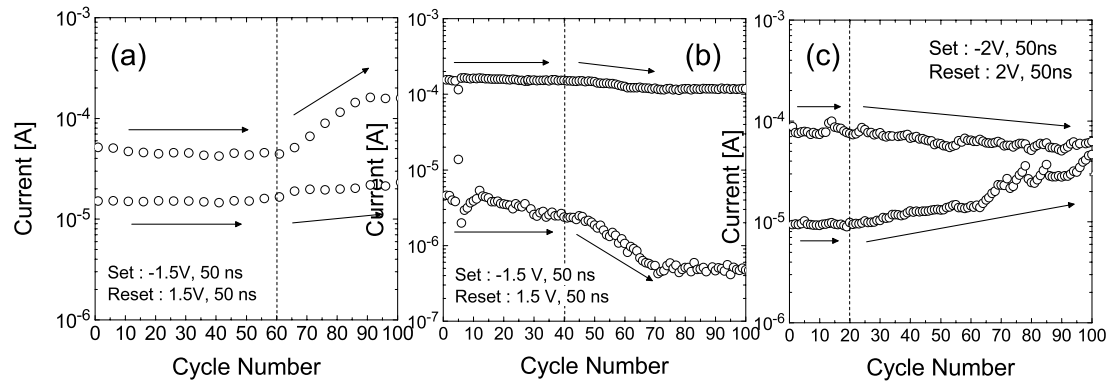


**Figure 2.** The variations of switching currents with the number of resistance switching cycles ( $n_{cy}$ ). In (a) and (b) the same switching voltages of +1.5 V (for the reset) and –1.5 V (for the set) were used, while in (c) the reset and set voltages were set to +2 V and –2 V, respectively. For all the cases, pulse width was fixed at 50 ns and the set and reset currents were read at +0.2 V after each pulse application.

be formed ( $\gtrsim 0.2$  eV) and carrier injection is limited. This corresponds to a much higher resistance of the layer, which can induce the field-driven migration of charged defects, so that the chance of having ionic switching becomes higher. It is believed that the former case corresponds to the present work, although the exact mechanism for incurring such a high density of defects is not well understood yet. Depending on the condition of various factors, possibly including URS compliance current and maximum reset current, sometimes an ionic mechanism (not an electronic mechanism such as SCLC) dominates even in the same sample, which will be a topic for our next report.

Under negative TE bias, the injected electrons from the TE fill in the traps while the current flows via the SCLC mechanism. The abrupt jump of the current level at  $\sim -1.1$  V in figure 1(a) and  $\sim -0.7$  to  $\sim -1.2$  V in figure 1(b) corresponds to the TFL in this case. As CC increases, the set state becomes more electrically conductive, suggesting that the traps have different energy levels and a higher CC induces trap filling with higher energy (figure 1(a)). During the reset process, the electrons that have filled the traps with higher energy detrapp more easily, allowing the reset to begin at a lower voltage (triangle symbol in figure 1(a)). Once the electrons detrapp from the trap sites, the subsequent carrier detrapping must occur at a higher voltage because the carriers trapped at higher energy levels detrapp first. This results in a more gradual reset process, as shown in the positive voltage regions of figure 1, which sometimes results in a negative differential resistance effect.

Once all of the traps become empty after application of positive voltage up to 1.4 V (figure 1(a)), the electrical conductivity of the reset state becomes identical irrespective of CC during the set process. Figure 1(b) shows the influence of maximum voltage during the reset process on the set step. As it increases, the onset negative voltage of the TFL decreases (i.e., absolute voltage increases). Here the CC during the set was fixed at 1 mA. Higher maximum reset voltage means more complete trap emptying during the reset process; thus, an even more negative voltage is necessary to induce the TFL transition. Therefore, figure 1 explains the general trend of electronic bipolar

switching in this electronic RS system by means of carrier trapping/detrapping asymmetric with respect to the bias polarity. The CC-dependent trapping and gradual detrapping can be used to induce the multi-level RS system, but their somewhat randomized nature generally inhibits their widespread use. This can be understood clearly from the following.

The switching uniformity and endurance are then discussed in conjunction with the trap configurations and their filling/emptying processes. For the switching uniformity/endurance test, the pulse switching system was used to induce the set and reset operations. Figure 2 shows two representative cases, one in which the set/reset current ratio increases as the number of RS cycles ( $n_{cy}$ ) increases ((a) and (b)), and another in which it decreases with  $n_{cy}$  (c). For (a) and (b) the same switching voltages of +1.5 V (for the reset) and –1.5 V (for the set) were used, while for (c) the reset and set voltages were set to +2 V and –2 V, respectively. For all cases, pulse width was fixed at 50 ns and the set and reset currents were read at +0.2 V after each pulse application.

Figures 2(a) and (b) show the random nature of the RS even for the given switching conditions. For an unidentified reason, the sample in figure 2(a) has a less conducting set state (low set current) at the beginning. Up to an  $n_{cy}$  of 60, the RS remains stable, but after that point, the set state current increases with the  $n_{cy}$  and eventually becomes saturated at an  $n_{cy}$  of  $\sim 90$ . The reset state appears to be influenced as well but to a lesser extent. On the other hand, in figure 2(b), the reset state undergoes a substantial change at an  $n_{cy}$  of  $\sim 40$ , at which value the reset state current decreases rapidly along with  $n_{cy}$  and becomes saturated at an  $n_{cy}$  of  $\sim 70$ . In this case, the set state was more conductive from the beginning and the set state was only marginally influenced. In figure 2(a), the increase in the set current at an  $n_{cy}$  of 60 can be understood from the following. As mentioned above, the bipolar RS region between the TE and the BE is composed of two parts: the trap-mediated RS region, which is located close to the anode interface region with a lateral dimension of several tens of nanometers and a depth dimension  $\lesssim 20$  nm, and residual Magnéli phase CF extending to the cathode interface. (See figure 3 of [7].) Therefore, the applied pulse voltage during

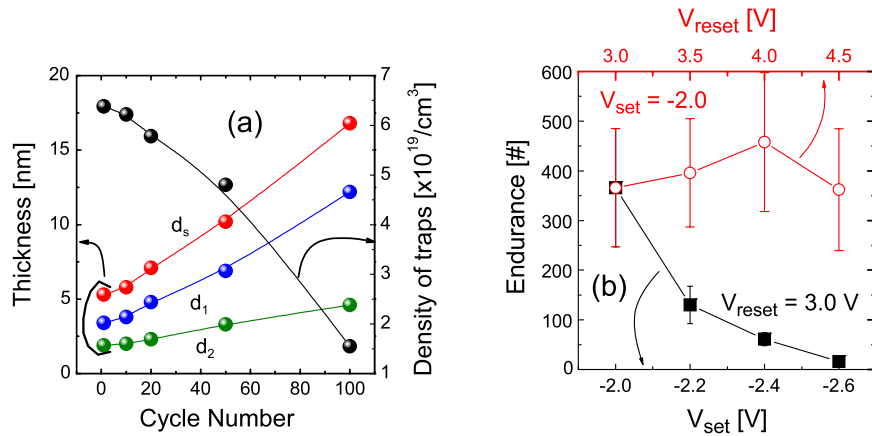


**Figure 3.** (a) The computed changes in  $d_1$ ,  $d_2$ ,  $d_s$ , and trap density ( $N_t$ ) as a function of the number of cycles ( $n_{\text{cy}}$ ) up to  $n_{\text{cy}} = 100$ . (b) The variation in endurance number with the various  $V_{\text{set}}$  and  $V_{\text{reset}}$  values. For varying  $V_{\text{set}}$  and  $V_{\text{reset}}$ , the  $V_{\text{reset}}$  and  $V_{\text{set}}$  values were fixed at 3.0 and  $-2.0$  V, respectively.

the RS was shared by the two parts. When the resistance of the switching region decreases for some unidentified reason, the voltage applied to that region decreases during the subsequent reset step because the resistance of the residual Magnéli phase CF remains constant. This results in less effective detrapping of the trapped carriers, which can be understood from the slightly increased reset current after the  $n_{\text{cy}}$  of  $\sim 60$  in figure 2(a). When the subsequent set pulse was applied to induce the carrier trapping, incomplete detrapping in the previous reset step induced trap filling at a slightly higher energy level. This further increases the conductivity of the set state. In the subsequent reset step, the detrapping becomes even less effective due to the further decreased voltage at this stage. Therefore, during the next set step, the traps with even higher energy levels are now filled and have an even higher set current flow. This appears to repeat until the uppermost trap level reaches an  $n_{\text{cy}}$  of  $\sim 90$  (figure 2(a)), and no further changes are observed.

A slightly different situation is observed in figure 2(b). Again, for the rather stochastic nature of the unipolar reset step, the set state appears to correspond to the state in which all the traps are already filled (highest set state current from the beginning). In this case, the resistance contrast is higher than that in figure 2(a), suggesting a larger portion of the switching region over the residual Magnéli phase CF. At an  $n_{\text{cy}}$  of  $\sim 40$ , the reset state current decreases rather abruptly due to more effective detrapping. Once this happens, the resistance of the switching region increases while that of the remaining Magnéli phase CF remains constant. During the subsequent set pulse application, there might be slightly insufficient trap filling, as can be understood from the slightly decreased set current after an  $n_{\text{cy}}$  of  $\sim 40$  (figure 2(b)). The subsequent reset then becomes more effective due to the even further increased voltage (increased voltage drop over the RS region) of the switching region, which further decreases the reset current. This pattern repeats until all of the carriers are detrapped at an  $n_{\text{cy}}$  of  $\sim 70$  (figure 2(b)). Therefore, the minimum reset current level shown in figure 2(b) corresponds to the complete trap emptied state, which induces a maximum set/reset current ratio ( $\sim 300$  in this case). In both cases, the RS ratio increases with  $n_{\text{cy}}$ , which is less problematic.

However, in figure 2(c), a much more problematic situation is shown, where the current ratio decreases continuously as  $n_{\text{cy}}$  increases due to the decreasing and increasing set and reset current, respectively. This finding indicates that the slightly higher set and reset pulse voltages in this case induce certain changes in the configuration of the ionic (or atomic) state of the switching region, which works as the framework for the electronic bipolar switching. The framework for the electronic bipolar switching was mentioned above, and a more detailed explanation is given below to explain the RS degradation shown in figures 2(c) and 3(b) (see [7] for even more details). The switching region is composed of densely arranged carrier traps. In addition, there is an asymmetric potential barrier between the trap-containing region (the thickness of which is referred to as  $d_1$ , having a lower average potential) and a relatively trap-free region (the thickness of which is referred to as  $d_2$ , with a higher average potential) [7]. Therefore, in this framework, the key parameters that govern the RS behavior include the trap densities ( $N_t$ ) and the asymmetric potential barrier height, which are intimately correlated [7]. The degraded set/reset current ratio implicitly means that  $N_t$  decreases as  $n_{\text{cy}}$  increases. Since the current transport follows the SCLC mechanism, the important parameters describing the switching region properties can be extracted from the fitting of the  $I$ - $V$  curves to the SCLC model. Here the  $I$ - $V$  curves after each reset pulse application were measured in the positive voltage region and fitted with a double layer SCLC model including discrete trap distributions to extract the various parameters (figure 3(a)). It should be noted that both  $d_1$  and  $d_2$  increase while  $N_t$  decreases with increasing  $n_{\text{cy}}$ , which eventually degrades the set/reset current ratio (figure 2(c)). The  $N_t$  decrease strongly suggests that (oxygen) ions migrate during the repeated switching, even though the sample is meant to operate in the electronic switching regime. The decrease of  $N_t$  with  $n_{\text{cy}}$  suggests that some of the oxygen vacancies in the trap layer disappear during switching. This finding means that the repeated set or the reset pulse (or both) drives the vacancies from the switching region.

In order to more clearly understand which step has the most influence on this degradation (drive-out of oxygen

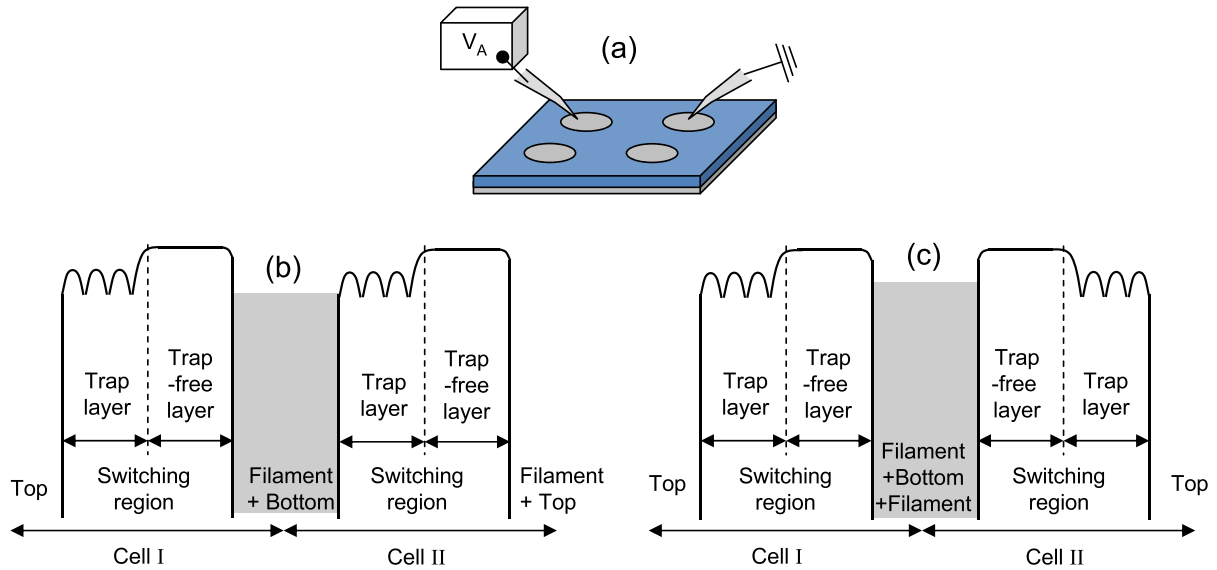


**Figure 4.** (a) Measurement configuration. (b) Serial connection is one possible structural configuration. (c) Anti-serial connection is the other possible configuration. The filament region and the common bottom electrode work as the connecting wire between the two structures.

vacancies from the RS region), the endurance was tested with different set and reset pulse amplitudes. Here the endurance was defined as the  $n_{cy}$  in which the set/reset current ratio decreases to 10% of its starting value. When the set pulse voltage ( $V_{set}$ ) changed, the reset pulse voltage ( $V_{reset}$ ) was fixed at 3.0 V, while  $V_{set}$  was fixed at  $-2.0$  V when the  $V_{reset}$  varied. Figure 3(b) shows the endurance test results, in which varying  $V_{reset}$  values had minor influence on endurance, suggesting that the refilling of oxygen vacancies with oxygen ions was not induced during the reset step. On the other hand,  $V_{set}$  has substantial influence on endurance; the larger the  $V_{set}$ , the smaller the endurance. This finding suggests that the oxygen vacancies become filled with the oxygen ions supplied from the TE (or even from the atmosphere) during the set switching because the negative bias was applied to the TE during the set switching. This naturally raises the question of why the reset process does not induce the vacancy annihilation, because there could be sufficient oxygen source from the neighboring  $TiO_2$  film or remaining CF. This question can be tentatively answered by considering that the peak current flows during the set switching. Although the oxygen ion migration is mainly driven by the electric field, it is still thermally enhanced [3]. Therefore, the peak current flow at the moment of set switching can induce a sufficient Joule heating effect that cannot be expected during the reset switching, and this effect enhances the directional motion of the oxygen atoms or ions from the TE to the vacancy sites in the switching region, even with symmetric pulse voltage application.

This conclusion invokes an idea about how to improve endurance; the excessive energy during the set switching should be minimal for achieving better endurance. One way to achieve this goal is to anti-serially connect the two RS cells, allowing one to become reset while the other becomes set under the given voltage pulse. Using this configuration, the peaking set current of one cell can be limited by the

high resistance of the opposite resetting cell. To test this idea, several RS cells with different configurations were fabricated on the same sample as shown in figure 4(a). Here, the MIM cell was first electroformed and reset by a unipolar switching with positive bias being applied to the TE. This results in a CF ruptured region that will work as the switching region during the subsequent bipolar switching near the TE. The same procedure was performed on a second cell to create another bipolar RS cell with a configuration similar to that of the first cell. For the third MIM cell, the same unipolar switching was performed with a negative bias on the TE, resulting in a ruptured CF region near BE. There can be one further control parameter that induces different RS behaviors, even in anti-serial cells, which is the different CC level during electroforming resulting in a different trap density. In short, the higher the CC is, the higher the trap density.

One can now measure the bipolar switching properties of MIM–MIM serially connected cells with the same directionality (serial cell; figure 4(b)) by contacting the first and third cells or opposite directionalities (anti-serial cell; figure 4(c)) by contacting the first and second cells.

Figure 5(a) shows the bipolar switching  $I$ – $V$  curves of the serially connected MIM–MIM structure. The hysteretic bipolar switching curve is identical to that of the single cell except for the double current jump (arrow, figure 5(a)) during the set process with the negative bias. This can be understood from the distribution of the two trapping regions (figure 4(b)). The inset figure in figure 5(a) shows the change in the set/reset current ratio of this serial structure as a function of  $n_{cy}$ . The endurance improved slightly compared with the single MIM, but it was still unsatisfactory.

Figures 5(b) and (c) show the bipolar switching  $I$ – $V$  curves of the anti-serial MIM–MIM when the two trap states (trap I and trap II) are identical and different, respectively. This can be achieved through controlling the CC during the electroforming step applied to each MIM. In contrast to the

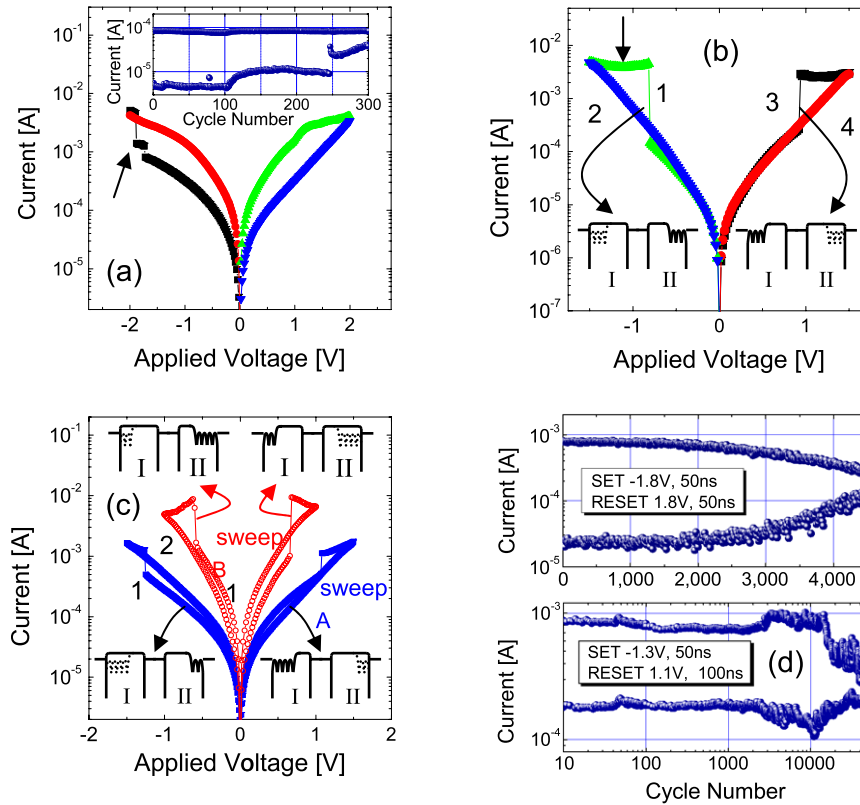


**Figure 5.** (a) Switching current–voltage ( $I$ – $V$ ) curves for the serial connection configuration. The inset shows the endurance result of this connection with  $-2$  V (50 ns) and  $2$  V (50 ns) for set and reset, respectively. (b) Switching  $I$ – $V$  curves for the anti-serial connection configuration with the same trap state in each cell. (c) Switching  $I$ – $V$  curves for anti-serial connection configuration with a different trap state in each cell. Sweeps A and B show the case of  $d_1^I > d_1^{II}$  and  $d_1^I < d_1^{II}$ , respectively. (d) Improved endurance result of the anti-serially connected MIM–MIM structure. The upper graph corresponds to the measurement setup with symmetrical set/reset pulses ( $-1.8$  and  $+1.8$  V with 50 ns duration), while the lower graph corresponds to the configuration with asymmetrical set/reset pulses ( $-1.3$  V/50 ns and  $+1.8$  V/100 ns).

single MIM or serial MIM–MIM structures, the current jump occurs in both polarities, suggesting that the TFL of the two trap regions occurs at the opposite bias polarity. To understand these  $I$ – $V$  curves, figures 5(b) and (c) show a schematic band structure of the connected structures. In these schematic figures, the dots indicate the carrier-filled trap sites.

For figure 5(b), the initial band structure is shown on the right-hand side when the  $I$ – $V$  sweep begins from 0 V and moves into the negative bias direction (curve 1); the trap-I layer is empty and the trap-II layer is filled with electrons because it had previously been positively biased. Therefore, the total current is governed by the trap-I layer. With decreasing bias voltage into the negative voltage range, the trap-I layer becomes filled with electrons. At the negative set voltage ( $V_{\text{set}}^B$ , which corresponds to  $V_{\text{TFL}}$  of trap I), every trap in the trap-I layer is filled and a current jump occurs. After this event, the trap-II layer becomes devoid of electrons during the further bias decrease, which results in a negative differential resistance (vertical arrow, figure 5(b)). Once a sufficiently negative voltage is reached, the trap-II layer becomes empty, and increasing the bias voltage back to 0 V results in curve 2. In this case, the resistance must be governed by the trap-II layer. Curve 2 must trace curve 1 almost precisely in  $V > V_{\text{set}}^B$  due to the identical resistance of the trap-I and trap-II layers. When a positive bias voltage is

applied, an inverse situation occurs in the trap-I and trap-II layers, showing symmetric  $I$ – $V$  curves of the negative bias case (curves 3 and 4). Due to the symmetry between the trap-I and trap-II layers, there is no difference in resistance under either polarity; hence, there is no memory effect. Therefore, the different resistances of the trap-I and trap-II layers should and did induce a memory effect (figure 5(c), asymmetric trap configuration).

There can be two different cases, even for the anti-serial, asymmetric trap configuration: the resistance of the (empty) trap-I layer is larger than that of the (empty) trap-II layer, or vice versa. Here the different trap region resistances are simply represented as the thickness of the trap layers ( $d_1$ ): larger  $d_1$  means higher resistance. These were confirmed from the resistance measurements of each MIM. Sweep A in figure 5(c) corresponds to the case in which trap I is more resistant than trap II ( $d_1^I > d_1^{II}$ ). The higher resistance of trap I is also induced by higher trap density rather than wider thickness, but here it was represented as wider thickness for the sake of convenience. For curve 1 of sweep A, the more resistant trap-I layer is empty, which results in high total resistance. After the current jump, the trap-I layer becomes filled with electrons, and a further sweep into the more negative bias empties trap II. This trap II has lower resistance than trap I. Therefore, curve 2 shows a higher

current level than curve 1, which achieves a memory effect. The memory effect of sweep A under a positive bias voltage occurs similarly. Sweep B in figure 5(c) corresponds to the case in which trap II is more resistant than trap I ( $d_1^I < d_1^{II}$ ). Therefore, after the current jump in curve 1 of sweep B, the total resistance becomes higher and a lower current level was achieved in curve 2. The switching  $I$ - $V$  curves in the opposite bias region are also similar. Therefore, the memory effect can be achieved for both cases provided that the resistances of the trap-I and trap-II layers are not identical. It should be noted that the total trap density (trap I + trap II) differs for sweeps A and B, which results in a generally different resistance.

The most remarkable feature of these anti-serially connected trap layers with different density is its highly improved switching endurance characteristics, which were optimized via proper adjustment of the trap distributions in the two MIMs. Figure 5(d) shows two of the best results. The upper graph of this figure shows that the cyclic endurance performance was improved by  $>15\times$  compared to what was observed in the previous cases and a larger resistance ratio was achieved. Here, symmetric pulse voltages of +1.8 and -1.8 V with a pulse duration of 50 ns were used to set and reset, respectively, the MIM-MIM structure with the anti-serial configuration. This improvement can be understood by comparison of the  $I$ - $V$  sweep curves with that of the single MIM or serial MIM-MIM.

As discussed previously, degradation of the set/reset resistance ratio was induced by a decrease in  $N_t$  resulting from the enforced filling of oxygen vacancies ( $V_O$ ) in the trap layer as described in figure 2. This filling process is induced by the negative bias to the top electrode and is accelerated by Joule heating from the electron current flow. This Joule heating effect must be the most serious at the moment of the current jump (peak temperature due to the high current pulse for a very short period of time) at a negative  $V_{set}^B$ . For the single MIM and serial MIM-MIM cases, the current jump occurs only under a negative bias, resulting in a unidirectional net oxygen migration. However, for this anti-serial MIM-MIM structure, the current jump occurs at both polarities, making the oxygen ion drift bidirectional, which suppresses the monotonic decrease in  $N_t$  as  $n_{cy}$  increases, resulting in better endurance.

The above discussion suggests that the switching voltage should be reduced to minimize the ionic motion to improve the endurance. Furthermore, the upper graph of figure 5(d) shows that the degradation was more severe for the reset state, suggesting that the reset voltage should be reduced to below that of the set voltage. The lower graph of figure 5(d) shows the best endurance performance obtained in the tests using -1.3 V/50 ns for set and +1.1 V/100 ns for reset. The current ratio was maintained in up to 45 000 cycles.

As a final comment, it was noted that the switching  $I$ - $V$  sweep curve of the anti-serial MIM-MIM structure should have been completely different from what was actually observed if it resulted from the ionic bipolar switching mechanism. For the ionic bipolar switching in the Pt/TiO<sub>2</sub>/Pt structure, in which both interfaces are actively involved in the accumulation and depletion of oxygen vacancies (note that

this is a situation different from what was shown in [10], where only one interface is involved in the switching), the  $I$ - $V$  sweep curves were expected to be repeated reversals of rectifying the  $I$ - $V$  curves with set-only switching behavior, which is certainly not the case here.

#### 4. Conclusion

In conclusion, the electronic bipolar resistive switching and its degradation in the Pt/TiO<sub>2</sub>/Pt structure are closely related to distribution of traps (most likely oxygen vacancies) and its variation with the switching cycles in the localized switching region of the memory cells. The electronic bipolar switching was induced from the asymmetric trap distribution within the CF rupture region near the anode interface formed during its unipolar reset operation. The imbalanced migration of oxygen accompanied by electronic switching significantly degrades the device endurance. The oxygen vacancy migration was more serious during set switching due to the enhanced Joule heating effect at the moment of set switching. Instead, the anti-serial connection of the Pt/TiO<sub>2</sub>/Pt cells resulted in substantial endurance improvements in which the concurrent occurrence of set and reset switching in the two opposite cells practically limited the excessive power dissipation, which enhances endurance. In general, the reduced switching power, for both set and reset operations, improved the endurance. However, this also invokes a concern about the sufficient set/reset current ratio. In addition, the anti-serial distribution of the traps within a single MIM cell should be realized to make use of this anti-serial strategy. This will be reported in subsequent works.

#### Acknowledgments

This study was supported by the National Research Program for the Nano Semiconductor Apparatus Development sponsored by the Korea Ministry of Knowledge and Economy (10034831) and the Converging Research Center Program through the National Research Foundation of Korea (2011K000610).

#### References

- [1] Waser R and Aono M 2007 *Nature Mater.* **6** 833
- [2] Lee M J *et al* 2007 *Adv. Mater.* **19** 3919
- [3] Kim K M, Jeong D S and Hwang C S 2011 *Nanotechnology* **22** 254002
- [4] Choi B J *et al* 2005 *J. Appl. Phys.* **98** 033715
- [5] Jeong D S, Schroeder H and Waser R 2007 *Electrochem. Solid-State Lett.* **10** G51
- [6] Lee M H, Kim K M, Kim G H, Seok J Y, Song S J, Yoon J H and Hwang C S 2010 *Appl. Phys. Lett.* **96** 152909
- [7] Kim K M, Choi B J, Lee M H, Kim G H, Song S J, Seok J Y, Yoon J H, Han S and Hwang C S 2011 *Nanotechnology* **22** 254010
- [8] Kim K M, Kim G H, Song S J, Seok J Y, Lee M H, Yoon J H and Hwang C S 2010 *Nanotechnology* **21** 305203
- [9] Kwon D H *et al* 2010 *Nature Nanotechnol.* **5** 148
- [10] Yang J J, Pickett M D, Li X, Ohlberg D A A, Stewart D R and Williams R S 2008 *Nature Nanotechnol.* **3** 429